POLITECNICO DI TORINO

Master's Degree in Mechatronic Engineering
Dipartimento di Automatica e Informatica

Master's Degree Thesis

3U CubeSat AODCS with Thruster Allocation

Supervisors

Prof. Elisa Capello

Prof. Hyeongjun Park

Candidate

Dario d'Angella

2022

Abstract

The accomplishment of a space mission depends on numerous aspects. Regarding spacecraft systems, the characteristic that makes the mission more difficult is that they must operate autonomously, or with few humans' assistance, in real time. Thus, an optimal management of the fuel consumption is necessary to ensure a longer mission's life.

Nowadays nanosatellites, such as CubeSat, are often used due to their limited cost, versatility, and capability to be assembled in a module which makes them perfectly suitable for various kind of space missions. The reduced size leads to a drawback: the impossibility to store a large amount of fuel. Especially, when the fuel consumption management becomes a crucial feature, a control allocation algorithm is used for this purpose since it can allocate the thrust force needed to accomplish a specific maneuver giving the best distribution of the command activity over the thrusters that are mounted on the spacecraft and this leads directly to a more efficient fuel usage.

Using a real thruster configuration, the goal of this thesis is to develop a control allocation algorithm and to implement it in a way to reduce the computational effort, and so to be adopted in a real-time scenario. After the implementation of the proposed algorithm, due to the ON/OFF nature of the thrusters, a modulator is developed to simulate real case scenarios. The modulator is tuned to improve the fuel usage as well as the number of thruster firings accordingly to the constraints imposed by the cluster of thrusters.

The whole system is then tested in MATLAB/Simulink environment for a couple of different missions and analyzed its robustness and the effectiveness of the proposed allocation by comparing the results with a system without any control allocation and modulator. Extensive simulations are performed to test both the systems.

Index

Chapter 1

Introduction

1.1 Motivation and objective

The goal of this thesis is to design and test different algorithms for a control allocator to be applied in a space mission involving a 3U CubeSat. The criticality behind the use of a nanosatellite is the impossibility to store a large amount of fuel so the management of the fuel consumption becomes one of the most important aspects to consider. The control allocation allows to reduce the fuel consumption, being an algorithm that optimizes the redistribution of the command forces over the thrusters. The efficiency of the tested control allocators is demonstrated in a rendezvous maneuver of two 3U CubeSats that have different thrusters' configurations, one involving an ideal 6-thrusters cluster and the other one a more realistic arrangement of seven thrusters.

The rendezvous approach is divided into more phases: launch, phasing, far range rendezvous, close range rendezvous and mating. This thesis will cover only the far range rendezvous and the close-range rendezvous. Due to the rotation of the Earth and the intrinsic limitations of the launching site, there is only one opportunity per day to launch a spacecraft into the desired orbit plane. The launch window depends on how much the spacecraft is capable to correct the plane differences right after the lift-off deriving from a deviation from the nominal launch time. The remaining differences are then corrected during the phasing and the rendezvous. After the launch, the chaser is ejected into the target orbital plane, usually in a lower orbit. During the phasing, the chaser should reduce the phase angle, i.e., the angle between the chaser and the target. The phasing is followed by the rendezvous. During these phases it is used a target centered frame and the motion of the chaser is described with respect to the target, instead of using an Earth centered frame like in the previous phases. The rendezvous marks a switching from absolute to relative navigation measurement of the states. During the far range rendezvous, the chaser reaches the target orbit. There may be a constraint on the final position that the chaser can occupy at the end of this maneuver. The purpose of the close-range rendezvous is to bring the chaser in a suitable position, with an acceptable velocity, attitude and angular rates for the mating respecting the constraint imposed by the safety approach corridor. If the mating axis is not along the V-bar direction, during the closing phase there is a fly-around maneuver that allows the acquisition of the approach axis [1]. In this thesis the far range rendezvous is accomplished by a Hohmann transfer which brings the chaser to a closer orbit reducing also the distance between the two satellites along the V-bar and stabilizing the chaser in a station-keeping point behind the target, making then possible the start of the close-range rendezvous, which in this presentation is implemented with a series of radial boosts.

1.2 Literature Review

1.2.1 CubeSat

CubeSat is a small satellite, specifically, due to its dimensions, it belongs to the category of the nanosatellite. It consists in a cube of size 10 cm x 10 cm x 10 cm which is also referred to as unit and a satellite composed by only one unit is called 1U CubeSat. These units can be assembled to create satellite different in size according to the purpose of the mission. So far, the biggest one is a 27U CubeSat which size is 34 cm x 35 cm x 36 cm [2]. The most used type is the 3U CubeSat which is also the smallest one that can fit a good amount of technology payloads to be tested or used for a total weight of 3-4 kg.

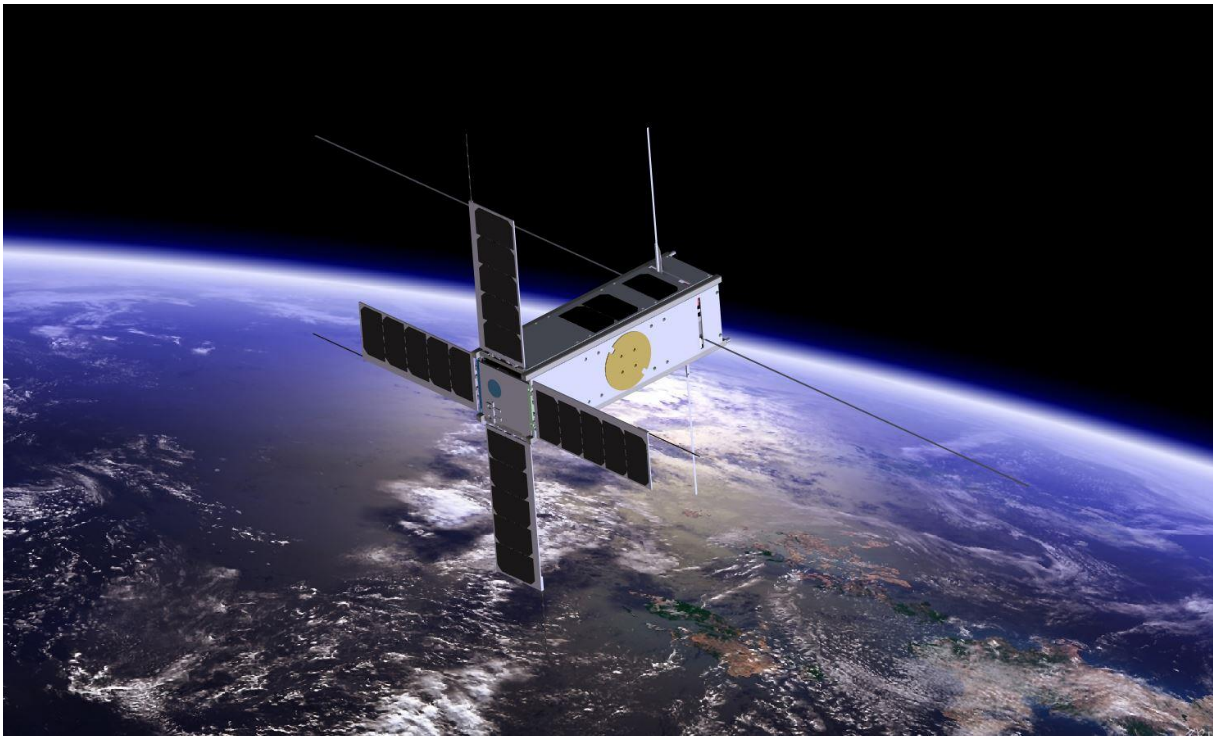

Figure 1.1 - PICASSO 3U CubeSat [3]

For instance, there are several ESA funded missions that involved the use of a 3U CubeSat to test different technologies and equipment, such as: GOMX-3, to demonstrate the reception of ADS-B signal and the quality of geostationary telecommunication satellite based on spot beam signal; QARMAN, to demonstrate re-entry technology such as new heatshield materials, the transmission of telemetry data during this phase of the mission and the deployment of a new passive aerodynamic drag stabilization system; SIMBA, to measure the Total Solar Irradiance and Earth Radiation Budget and to demonstrate the efficiency of a new precise pointing system; Picasso, to measure Stratospheric Ozone distribution, Mesospheric Temperature profile and the density of electron in the ionosphere; RadCube, to measure the space radiation and magnetic field in LEO [3]. The importance of these missions is that all of them have demonstrated the use of miniaturized technologies since the availability of payload is reduced due to the small size of the CubeSat.

This flexibility and adaptability are making CubeSat attractive not only to university purpose as it was in principle, but also to space agencies and most of all to companies. Most of the CubeSats nowadays deployed are used for Earth observation and communications since their reduced dimension allows the placement of a large number of satellites on the same vector making possible the creation of a dense constellation. An example was a 2017 Indian mission, PSLV-C37, which made the record of 104 satellites on the same launch vehicle, 101 of them were commercial international satellites. 103 out of 104 were CubeSats: 88 owned by Planet Labs, an American public Earth imaging company, 8 by Spire Global for vessel tracking and weather measurement services [4].

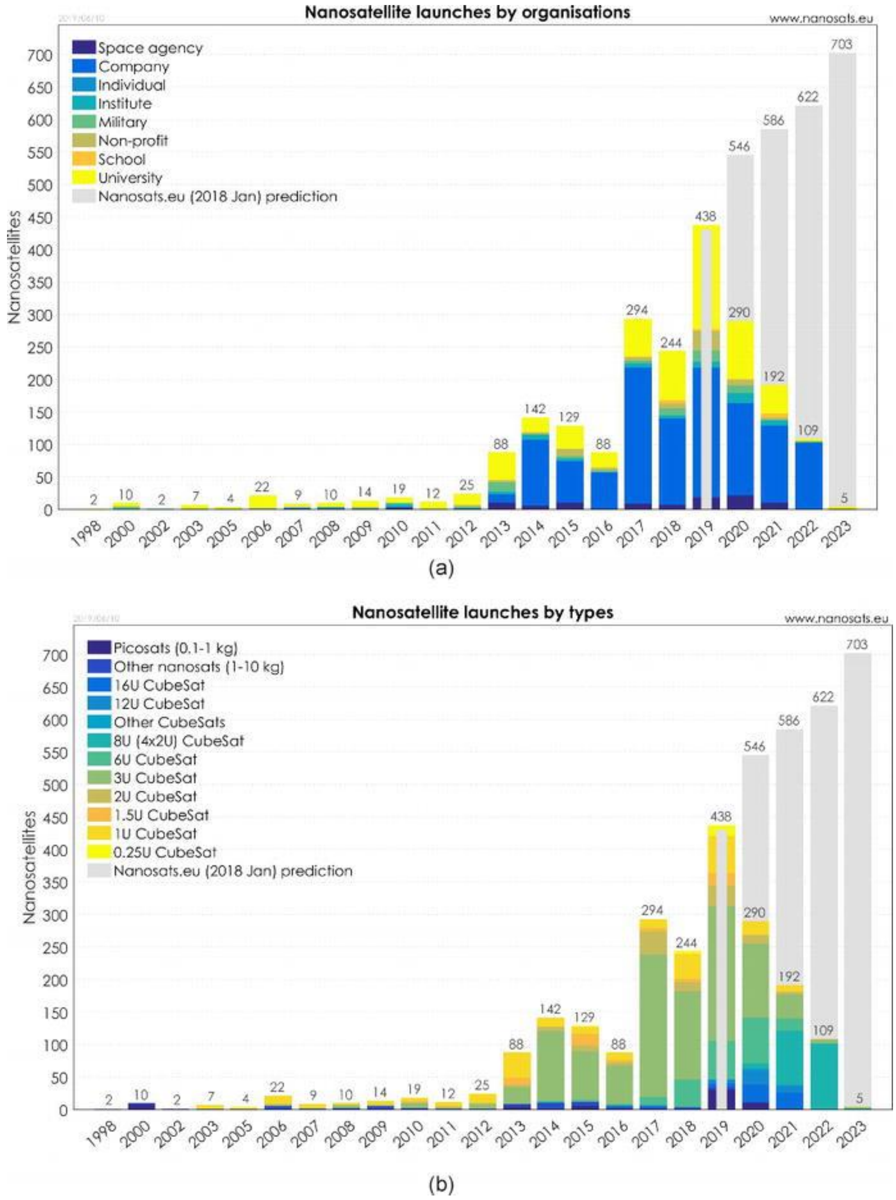

Figure 1.2 - Number of nanosatellites launched per year and (a) organization or (b) form factor [3]

Since most of the CubeSat are 10 cm x 10 cm regardless of length, they are allocated into a deployment system called Poly-PicoSatellite Orbital Deployer (P-POD). For CubeSat bigger than the 3U type, instead of using the standard P-POD, the satellite is placed in a special canister during launch so it can dispense the payload in the desired orbit. The developer of CubeSat and P-POD is the Cal Poly that through the CubeSat Program provides specifications and standards to all the users who are intended to use this technology giving also mandatory tests and validations to be done. The CubeSat Project started in 1999 with the purpose of making more accessible the satellite’s technology. The reduction of the cost and the time needed for the production have make more attainable frequent launches and so easier to reach the space. The standardization regards the design of the CubeSat, ranging from the 1U form to the 12U one, and the relative dispenser and interfaces in order to ensure a successful detachment of the canister from the launch vehicle without damaging it or the primary payload. The two main dispensers are: the already mentioned P-POD, which utilizes a rail-based design to deploy the CubeSat contained in it, and another one developed by Planetary Systems Corporation based on a tab design. Both of them have a spring inside that shoves a pusher plate responsible for the deployment force, the CubeSat glides along the rails (or the tabs) and reaches the orbit [5].

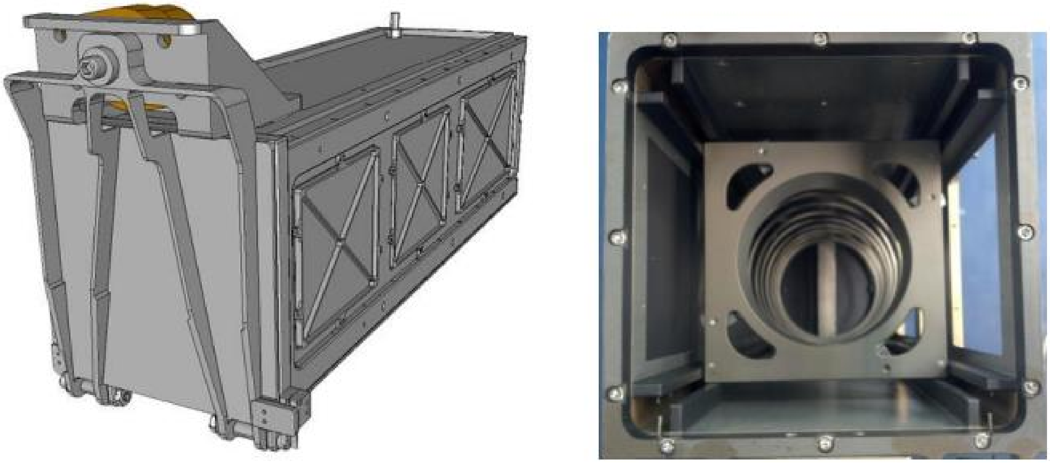

Figure 1.3 - P-POD representation and a cross section of it [4]

The deployment of the P-PODs in a launch vehicle (LV) is usually done as a secondary space mission’s objective. An example is the NASA mission InSight in which from the vector Atlas V 401 two 6U CubeSat where deployed.

This secondary mission, known as Mars Cube One (MarCO), is the first that has used CubeSat for interplanetary operation and its results have proven the capability of the CubeSat to operate in the deep space. The main goal of MarCO was to create a bent pipe communications for InSight during the EDL (entry, descent, landing) sequence on Mars, thus the two CubeSats, known as MarCO-A and MarCO-B, had to operate at a distance of ~1.4 AU demonstrating the capability of these small spacecraft to communicate and to correct their attitude, orientation and trajectory [6].

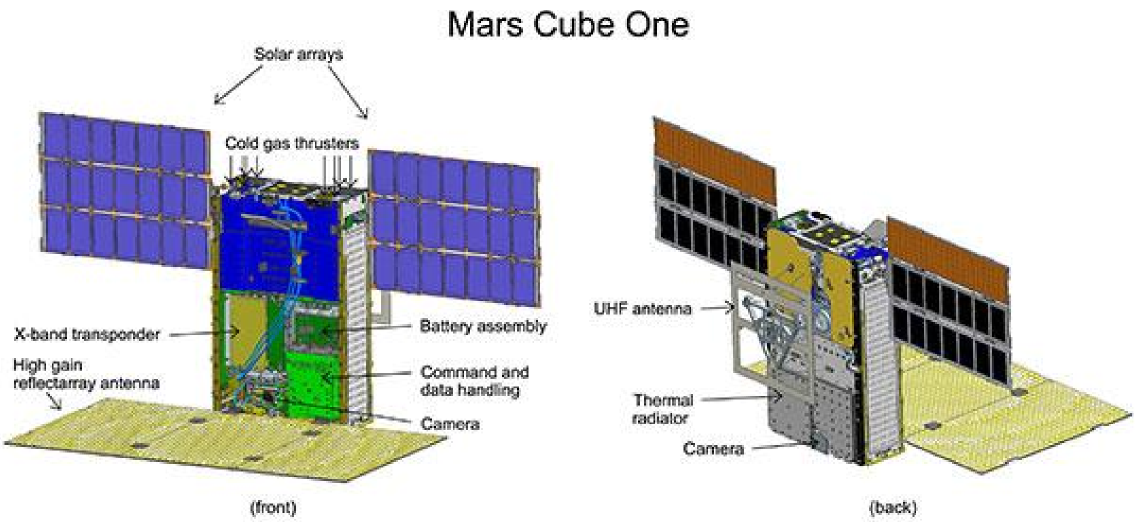

Figure 1.4 – Representation of a MarCo 6U CubeSat [7]

Until this mission, CubeSats were only deployed in low Earth orbit (LEO). The two small satellites flew independently, each of them was guided by a different team. They were identical to ensure redundancy in case of failure of one of them. They were equipped with two solar panels, a high-gain X-band antenna to transmit data to Earth and an ultra-high frequency (UHF) radio receiver in charge of receiving data from InSight during its descent to Mars. During the landing phase the antenna was pointing back to Earth while the receiver towards the lander. This system permitted the reception, the formatting and the relaying of the data stream almost in real-time [7].

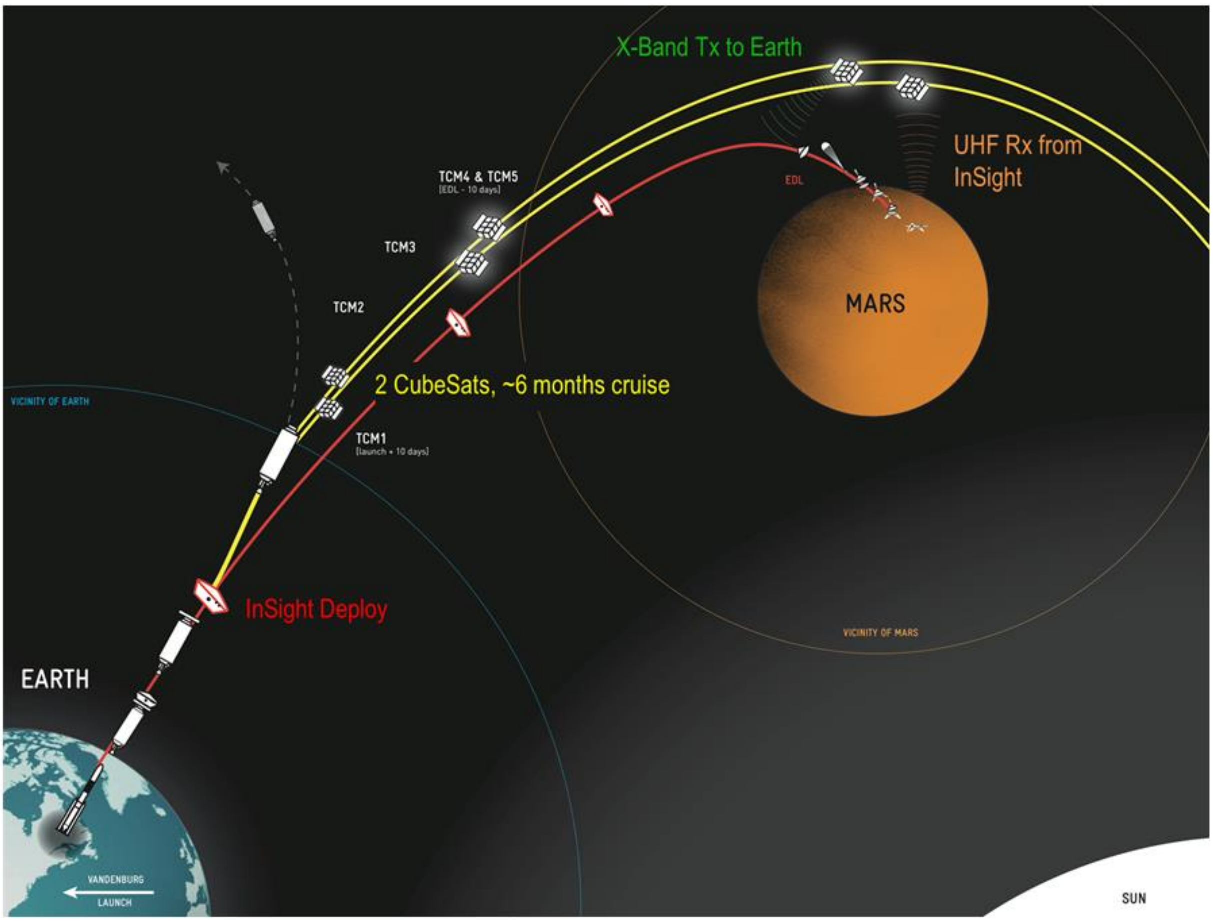

Figure 1.5 – Bent pipe communications created by MarCo-A and MarCo-B for the lander InSight [6]

1.2.2 Control Allocation

The control allocation's principle allows to separate the design of the controller from the design of the control allocator. Designing a controller means to find a suitable control law that represents the total control effort to be produced while the task of the control allocator is mapping the total control demand onto each actuator in such way that the total thrust forces generated by the cluster of thrusters is equal to the control demand. Depending on what is the purpose and most of all the resources in terms of on-board computer, it is possible to choose different control allocation algorithm.

Satellites are over actuated systems, it means that there are more actuators, i.e., the n-thrusters on the satellite, than controlled variables, i.e., the m-thrust forces generated along the three cartesian body axes of the satellite ($m = 3$), in order to ensure reliability. The control allocation is a mapping from the control vector $u \in R^n$ to the desired one $v_d \in R^m$ with $n>m$:

$$v_d = B\,u \tag{1.1}$$

where u is bounded by its upper and lower limits $u_{min} \leq u \leq u_{max}$ and B is a matrix in which each column represents how the associated thruster is oriented in space with respect to the body frame of the satellite. The upper and lower limits came from the physical constraints of the thruster. Usually there is more than one solution due to redundancy, control allocation is necessary since it finds the best distribution of the command activity over the actuators. In literature can be found a wide variety of control allocation algorithms that are used in aerospace and naval applications, for which it is used the same approach like in [8].

The simplest and widely used algorithm is based on the Moore-Penrose pseudo-inverse since, due to redundancy, the configuration matrix B is not square. Thus, the problem is:

$$u = [B^T(BB^T)^{-1}]v_d \tag{1.2}$$

This method is the fastest, but it does not allow to handle directly the saturation of the thrusters. There are some methods based on the pseudo-inverse which can be used to handle the saturation. Some examples can be found in [8], [9], [10], [11], [12]. In [9] is proposed a dynamic weight pseudo-inverse control allocation to allocates the desired control torque onto four reaction wheels. The weight coefficients are dynamic in the sense that they depend on the states of the reaction wheels, if they are far or near to saturate. The higher is the rotational speed the lower will be the weight factor meaning that a smaller control torque will be allocated to the corresponding reaction wheel. This will make harder for the actuator to reach the saturation. In [8], [10]-[12] is shown a technique called redistributed pseudo-inverse or cascading generalized inverses, which, in case of saturation, redistributes among the other actuators the commanded forces. It is an iterative process that stops when the commanded forces are entirely distributed, it means when no saturation occurs, or the number of iterations reaches its admissible maximum (n-m). For example, if the i-component of the control vector u exceeds its limit its forced to its maximum value (or minimum), its contribution is removed from the matrix B by removing the i-column and a new pseudo-inverse P' is calculated with the new reduced B matrix, called B'. A new desired vector v_d' is calculated by subtracting the contribution of the saturated actuator:

$$v_d' = v_d - B_i\, u_{i,max} \tag{1.3}$$

A new control vector u' is computed:

$$u' = P'v_d' \tag{1.4}$$

The iterations go on until the conditions exposed before are reached. For cases when in the end there are fewer than m actuators that do not saturate, this method results not effective and an approximation of it is used in which the saturated thruster that exceeds the limit with a close value it is not clipped and it is taken as good. Being an iterative procedure is more expensive in terms of computational cost than the normal pseudo-inverse or the dynamic weight pseudo-inverse. It is worth to notice that the dynamic weight pseudo-inverse can not be applied to thrusters that work in an ON/OFF manner since they can only assume 0 or u_{max} as working values. In [10] is also proposed an optimization using the quadratic programming (QP) as a quite effective way to handle the constraints with the advantage of being numerically simple.

A more efficient algorithm but also more expensive in terms of computational effort that considers the upper and lower limits is the linear programming (LP) optimization. The problem can be formulated as a minimization one:

$$
\begin{aligned}
&\min_{u} f^T u \\
&s.t. \quad \begin{cases} B\,u = v_d \\ u_{min} \leq u \leq u_{max} \end{cases}
\end{aligned}
\tag{1.5}
$$

where the vector f is a column vector of dimension n.

In [13] and [14] the limit of LP, i.e. the performance CPU needed to run the optimization which make difficult the application in a real-time scenario, is overcome by using a sub-optimal thruster allocation [12] or computing an off line optimal thruster combinations table [13]. Since the LP is based on two phases, the first consists in finding a basic feasible solution and the second an optimal one, in [12] the basic feasible solution is found using the grouping method as starting point for the second phase. In [13], using the simplex method applied to an LP optimization, an optimal thruster combinations table for all the obtainable moment is precompiled and then uploaded on the on-board computer. In real-time applications, according to the control command u and the table, the fire duration is calculated in the selected combination and the feasible one is the one with a non-negative duration. The feasible condition of the simplex method grants that if a solution is feasible is also optimal.

1.3 Overview of the thesis

Chapter 2

Modelling

This chapter covers the description of the satellite itself and its position and orientation inside different reference frames as well as the description of the mathematical models used to delineate the missions that the chaser must accomplish.

2.1 Reference Frames

The very first thing to do is to introduce the reference frames that describe, in a complete way, the motion and orientation of a satellite that is travelling in the proximity of the Earth.

2.1.1 Geocentric Equatorial (GE) Frame

It is an inertial frame in which its origin coincides with the geometric center of the Earth. Some assumptions and simplifications are made: the Earth is a perfect sphere with a homogeneous distribution of mass, this implies that the center of mass is the same of the geometrical center; the relative motions of the Earth such as the axial precession and the astronomical nutation are neglectable since we are dealing with small objects in orbits close to Earth and with short period of time. The axes of the frame, usually called $\hat{\boldsymbol{I}}$, $\hat{\boldsymbol{J}}$,$\hat{\boldsymbol{K}}$, follow the right-hand rule and are fixed. $\hat{\boldsymbol{I}}$ is the direction that goes from the center of the Earth to the center the Sun when the Earth passes through the vernal equinox, the first day of spring. $\hat{\boldsymbol{K}}$ coincides with the polar rotation axis and $\hat{\boldsymbol{J}} = \hat{\boldsymbol{I}} \times \hat{\boldsymbol{K}}$. Both $\hat{\boldsymbol{I}}$ and $\hat{\boldsymbol{J}}$ lie on the equatorial plane. In this frame are represented the position of both the target and the chaser, useful to the describe maneuver such as the Hohmann transfer as it will be explained later.

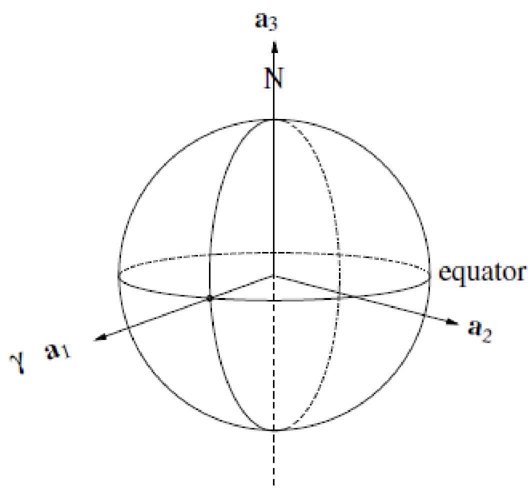

Figure 2.1 – GE frame [1]

In Figure 2.1 the $\boldsymbol{a}_1$ axis coincides with what it was previous called $\hat{\boldsymbol{I}}$, $\boldsymbol{a}_2$ with $\hat{\boldsymbol{J}}$ and $\boldsymbol{a}_3$ with $\hat{\boldsymbol{K}}$.

2.1.2 Local Vertical Local Horizontal (LVLH) Frame

It is a non-inertial reference frame. This frame is used for orbiting objects and for relative motion between different orbiting objects. In our case it is centered in the center of mass the target spacecraft which is flying in a circular orbit around the Earth. The $\boldsymbol{l_3}$ axis (local vertical) lies on the orbit plane and it is defined along the direction that goes from the target to the Earth. The local horizontal axis $\boldsymbol{l_1}$ is perpendicular to $\boldsymbol{l_3}$, lies on the orbit plane and it has sign concordant with the orbital velocity. In our case, since the orbit is circular and the Earth is located at the center of it, the local horizontal axis is tangent to the orbit. The orbit pole axis $\boldsymbol{l}_2 = \boldsymbol{l}_3 \times \boldsymbol{l}_1$ is perpendicular to the orbit plane.

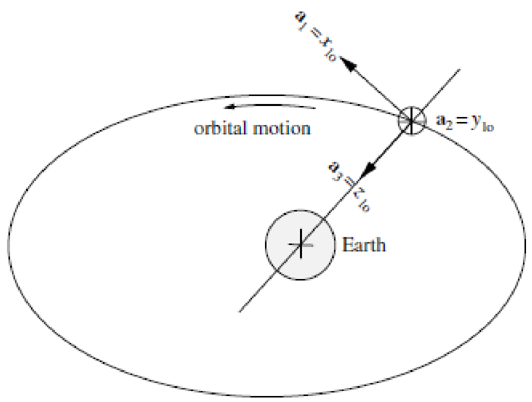

Figure 2.2 – LVLH frame [1]

In Figure 2.2 the $\boldsymbol{a}_1$ axis coincides with what it was previous called $\boldsymbol{l}_1$, $\boldsymbol{a}_2$ with $\boldsymbol{l}_2$ and $\boldsymbol{a}_3$ with $\boldsymbol{l}_3$.

2.1.3 Body Frame

It is fixed in the body center of mass. The center of mass is considered unchanging over time even if in a real scenario this is not true due to several reasons, for example the mass reduction due to the fuel consumption or the deployment of instruments that will affect the inertia of the spacecraft. In this thesis these effects are not considered. Since there is no convention over the body frame axes it is reasonable to consider them as principal axes of inertia. The $\boldsymbol{x}$ axis is aligned with $\boldsymbol{l_1}$ while $\boldsymbol{y}$ and $\boldsymbol{z}$ lie on the same plane perpendicular to $\boldsymbol{x}$.

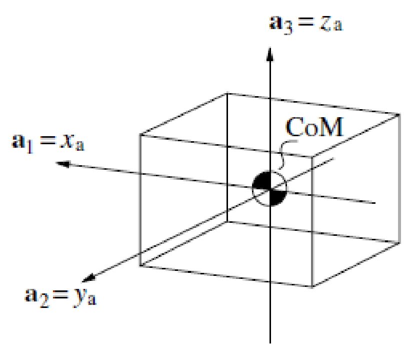

Figure 2.3 – Body frame [1]

2.2 Rotation Matrix

Once that the needed reference frames are defined, it is appropriate to introduce a transformation matrix that describes the rotation between two different frames. In this thesis's particular case, the motion of the body that represents the chaser satellite must be also expressed in the target satellite centered frame (LVLH frame). To fully describe a rotation between two objects or reference frames, three elemental rotations are needed. Using the Euler's angles representation, in particular the set of Tait-Bryan 321 Euler's angles, it is possible to reconstruct the orientation of the chaser's reference frame into the target's one. It is worth to mention that the order in which each rotation is executed is important since a different order will give a different resulting final rotation. Denoting the angles φ, θ and ψ (they represent respectively the yaw, the pitch and the roll), the rotation matrix will be:

$$M_B^{LVLH} = \begin{bmatrix} \cos\psi & -\sin\psi & 0 \\ \sin\psi & \cos\psi & 0 \\ 0 & 0 & 1 \end{bmatrix} \begin{bmatrix} \cos\theta & 0 & \sin\theta \\ 0 & 1 & 0 \\ -\sin\theta & 0 & \cos\theta \end{bmatrix} \begin{bmatrix} 1 & 0 & 0 \\ 0 & \cos\varphi & -\sin\varphi \\ 0 & \sin\varphi & \cos\varphi \end{bmatrix}$$

(2.1)

The typology of rotation used is an extrinsic yaw-pitch-roll rotation. It means that each rotation is around the original axes of the system.

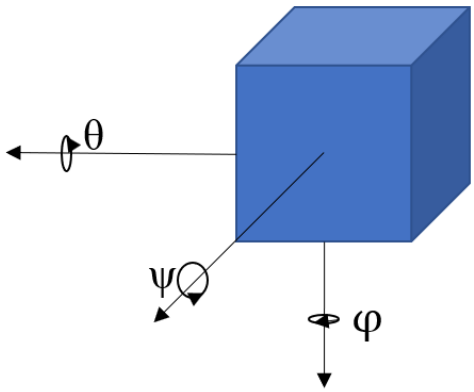

Figure 2.4 – Euler angles

The relation between the two reference frames is expressed by the following equation:

$$\begin{bmatrix} x_B \\ y_B \\ z_B \end{bmatrix} = M_B^{LVLH} \begin{bmatrix} x_{LVLH} \\ y_{LVLH} \\ z_{LVLH} \end{bmatrix}$$

(2.2)

The use of Euler's angles gives a direct and intuitive representation of what is the orientation of the object since it is easy to imagine, but this will also lead to a problem known as gimbal lock. Gimbal lock, in this representation, happens when the pitch angle θ reaches a value of $\pm\frac{\pi}{2}$.

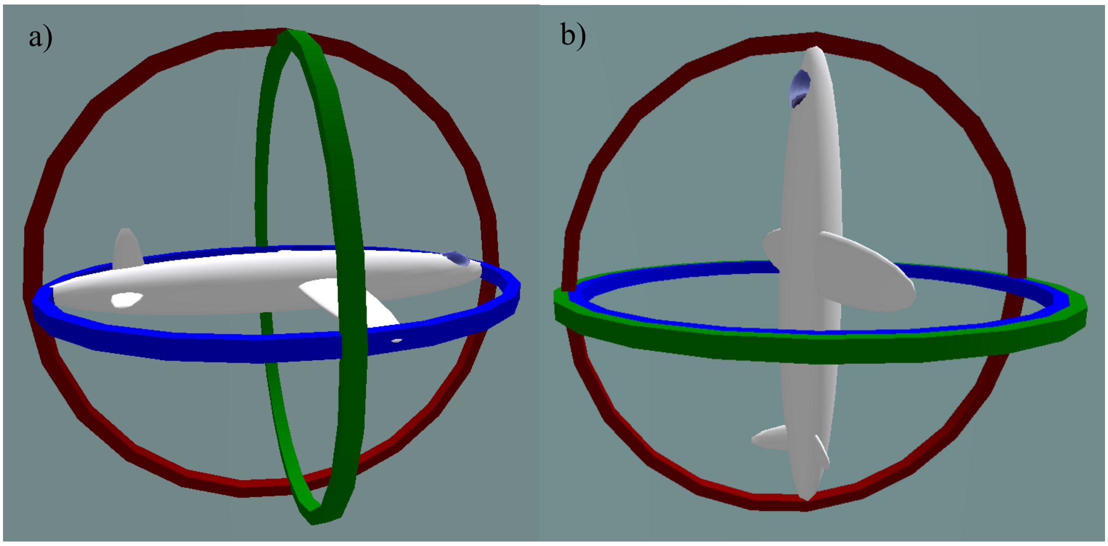

Figure 2.5 – a) normal situation [15] and b) gimbal lock in which one degree of freedom is lost [16]

Solving the matrix multiplications in (2.1):

$$M_B^{LVLH} = \\ = \begin{bmatrix} \cos\psi\cos\theta & \cos\psi\sin\varphi\sin\theta - \cos\varphi\sin\psi & \sin\varphi\sin\psi + \cos\varphi\cos\psi\sin\theta \\ \cos\theta\sin\psi & \cos\varphi\cos\psi + \sin\varphi\sin\psi\sin\theta & \cos\varphi\sin\psi\sin\theta - \cos\psi\sin\varphi \\ -\sin\theta & \cos\theta\sin\varphi & \cos\varphi\cos\theta \end{bmatrix}$$

(2.3)

Solving (2.3) for $\theta = \frac{\pi}{2}$ and doing some math:

$$M_B^{LVLH} = \begin{bmatrix} 0 & \sin(\varphi-\psi) & \cos(\varphi-\psi) \\ 0 & \cos(\varphi-\psi) & -\sin(\varphi-\psi) \\ -1 & 0 & 0 \end{bmatrix}$$

(2.4)

From the matrix (2.4), it can be noticed that when $\theta = \pm\frac{\pi}{2}$, φ and ψ lead to the same transformation so it is not possible to determine individually each angle but only their sum or difference. This situation of singularity leads to a loss of a degree of freedom.

Quaternions are used to overcome the problem given by the gimbal lock. A quaternion is a column vector composed of four elements, the first one is a scalar while the other three constitute the vectorial part of it:

$$q = \begin{bmatrix} q_0 \\ q_1 \\ q_2 \\ q_3 \end{bmatrix} = \begin{bmatrix} q_0 \\ q_v \end{bmatrix}$$

(2.5)

The elements of a quaternion are such that:

$$q_0^2 + q_1^2 + q_2^2 + q_3^2 = 1 \tag{2.6}$$

The new rotation matrix, expressed in quaternion, is the following:

$$M_B^{LVLH} = \begin{bmatrix} q_0^2 + q_1^2 - q_2^2 - q_3^2 & 2\,(q_1 q_2 - q_0 q_3) & 2\,(q_1 q_3 + q_0 q_2) \\ 2\,(q_1 q_2 + q_0 q_3) & q_0^2 - q_1^2 + q_2^2 - q_3^2 & 2\,(q_2 q_3 - q_0 q_1) \\ 2\,(q_1 q_3 - q_0 q_2) & 2\,(q_2 q_3 + q_0 q_1) & q_0^2 - q_1^2 - q_2^2 - q_3^2 \end{bmatrix} \tag{2.7}$$

Later in this thesis it is shown that the quaternion can be taken directly from the attitude kinematics of the spacecraft.

Since the quaternion does not give an immediate visualization and human-friendly representation of the attitude of an object, it is convenient to convert them into Euler's angles using the following formula:

$$\begin{bmatrix} \varphi \\ \theta \\ \psi \end{bmatrix} = \begin{bmatrix} atan2(2\,(q_0 q_1 + q_2 q_3), 1 - 2\,(q_1^2 + q_2^2)) \\ asin\,(2\,(q_0 q_2 - q_3 q_1)) \\ atan2(2\,(q_0 q_3 + q_1 q_2), 1 - 2\,(q_2^2 + q_3^2)) \end{bmatrix} \tag{2.8}$$

2.3 Spacecraft Model

For simplicity, the spacecraft can be approximately considered as a rigid body in which its center of mass is located in its geometric center throughout the entire duration of the simulation, this means that the distribution of the mass remains uniform and constant without considering the loss of fuel mass consumption. Without loss of generality, it is convenient to say that the three axes of inertia coincide with the three axes of symmetry of the rigid body. The satellites used in this thesis are two 3U CubeSats. This type of spacecraft is a parallelepiped of dimension 10 cm × 10 cm × 30 cm.

2.3.1 Attitude Dynamics

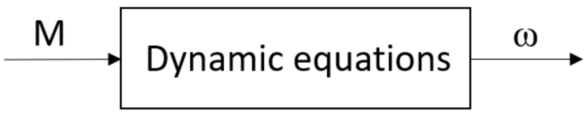

Figure 2.6 – The dynamic equations are a relationship between the moment acting on a body and its angular velocity

The dynamic of the spacecraft is given by its rotational motion. Due to the assumption of rigid body made before, the satellite can be considered as a continuous body in which each *i*-element of it maintains constant its distance r_i with respect to the center of mass.

The angular momentum that this kind of body that rotates at an angular velocity ω, is so defined:

$$H = \int_B r \times (\omega \times r) \, dm$$

(2.9)

The same formula can be written using a more convenient matrix notation using the inertia matrix.

$$I = \begin{bmatrix} I_{xx} & I_{xy} & I_{xz} \\ I_{yx} & I_{yy} & I_{yz} \\ I_{zx} & I_{zy} & I_{zz} \end{bmatrix}$$

(2.10)

For the simplification stated before, the axes of inertia are also principal so only the principal moments of inertia along the diagonal of the tensor exist.

$$I = \begin{bmatrix} I_x & 0 & 0 \\ 0 & I_y & 0 \\ 0 & 0 & I_z \end{bmatrix}$$

(2.11)

The final matrix form of the angular momentum is

$$H = I \, \omega = \begin{bmatrix} I_x & 0 & 0 \\ 0 & I_y & 0 \\ 0 & 0 & I_z \end{bmatrix} \begin{bmatrix} \omega_x \\ \omega_y \\ \omega_z \end{bmatrix}$$

(2.12)

From the second law of dynamics for a rotating body it is know that the overall moment acting on a body is

$$M = \dot{H}$$

(2.13)

Being

$$\dot{H} = I \, \dot{\omega} + \omega \times I \, \omega$$

(2.14)

The Euler moment equation is so obtained

$$M = I \, \dot{\omega} + \omega \times I \, \omega$$

(2.15)3

The purpose is to obtain ω as output having as input the moment M so it can be used later in describing the kinematic. Being the inertia tensor invertible, it is possible to rewrite the previous formula

$$\dot{\omega} = I^{-1} \left(M - \omega \times I \, \omega \right)$$

(2.16)

Through an integration in time is finally reached the solution.

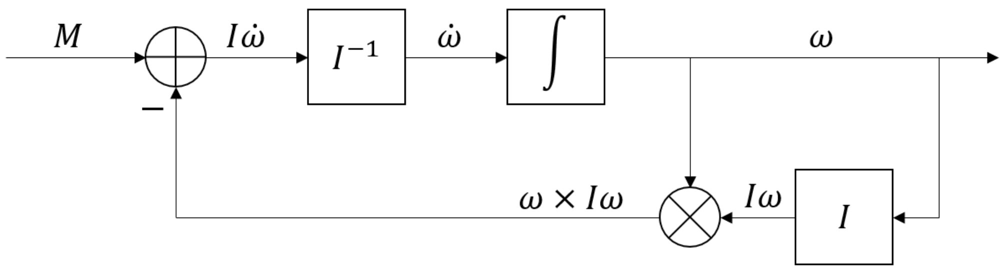

Figure 2.7 – Schematic block of the Euler equation

2.3.2 Attitude Kinematics

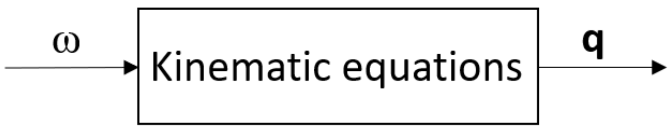

Figure 2.8 – The kinematic equations are a relationship between the angular velocity of the body and its attitude

The movement of the spacecraft is a roto translational movement composed by translations of the center of mass and rotations of the body around an axis passing through the center of mass. The kinematic equations establish a relationship between the angular velocity of the body ω and the Euler angles, or the corresponding quaternion.

For the reason expressed above, the use of quaternion is a more convenient option, considering also that the computational effort of computing its integration is less.

The evolution of the quaternion in time is so described:

$$\dot{q} = \frac{1}{2} q \otimes \omega^q$$

(2.17)

The vector ω^q represent the extension in four dimensions of the vector ω.

$$\omega^q = \begin{bmatrix} 0 \\ \omega_1 \\ \omega_2 \\ \omega_3 \end{bmatrix}$$

(2.18)

The quaternion product $q \otimes$ can be described as a 4×4 matrix:

$$q \otimes = \begin{bmatrix} q_0 & -q_1 & -q_2 & -q_3 \\ q_1 & q_0 & -q_3 & q_2 \\ q_2 & q_3 & q_0 & -q_1 \\ q_3 & -q_2 & q_1 & q_0 \end{bmatrix}$$

(2.19)

Since the first element of the vector ω^q is equal to 0, the kinematic equation is rewritten as:

$$\dot{\boldsymbol{q}} = \frac{1}{2} Q \, \boldsymbol{\omega}$$

(2.20)

Where Q is a modified version of the matrix $q \otimes$:

$$Q = \begin{bmatrix} -q_1 & -q_2 & -q_3 \\ q_0 & -q_3 & q_2 \\ q_3 & q_0 & -q_1 \\ -q_2 & q_1 & q_0 \end{bmatrix}$$

(2.21)

By integrating $\dot{q}$ is possible to obtain the attitude of the spacecraft.

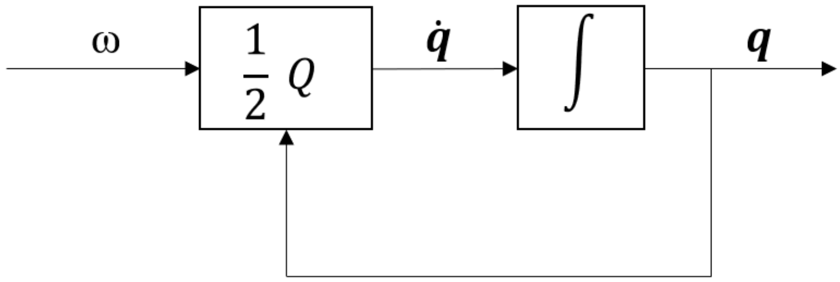

Figure 2.9 – Schematic blocks on the kinematic equation

2.4 Motion Dynamics

The scenario of the mission simulation involves two 3U CubeSats, a chaser and a target at two different low Earth orbits. The chaser starts from a lower orbit and after a rendezvous maneuver it approaches the target reaching a closer orbit to it. In doing so a relative motion between the two orbiting spacecrafts must be described. Since the distance between the two satellites can be considered small with respect to the distance of the chaser and the center of mass of the Earth, both the orbits are circular and the target is only subjected to the gravitational force, it is possible, among other describing formulations, to use the so-called Hill's equations.

The two bodies, considered as point masses, are immerged in the Earth's gravitational field so the force acting on them is a central force. Under these circumstances the Newton's law of gravitation can be applied:

$$\overrightarrow{F_g}(\vec{r}) = -G\,M\frac{m}{r^2}\frac{\vec{r}}{r} = -\mu\,\frac{m}{r^3}\,\vec{r}$$

(2.22)

In which G is the gravitation universal constant, M is the mass of the central object responsible for the gravitational field, in this case the Earth and so μ is the standard gravitational parameter associated with the Earth, m is the mass of the orbiting object, $\vec{r}$ represents the position vector of the object in the inertial frame.

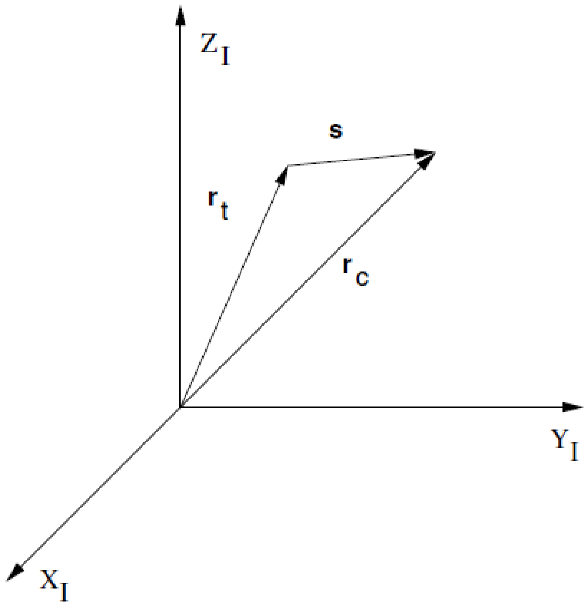

Figure 2.10 – Position vectors of the chaser and the target in the inertial frame [1]

In order to obtain the motion of both the satellites, the force is divided by the mass of the chaser m_c and the target m_t, which in this case are the same. Remembering that the target is only affected by the gravitational force and the chaser is affected also by the forces derived by the thrusters' action:

$$\ddot{\overrightarrow{r_t}} = -\mu\,\frac{\vec{r}_t}{r_t^3} = \overrightarrow{f_g}\,(\overrightarrow{r_t})$$
$$\ddot{\overrightarrow{r_c}} = -\mu\,\frac{\vec{r}_c}{r_c^3} + \frac{\vec{F}}{m_c} = \overrightarrow{f_g}\,(\overrightarrow{r_c}) + \frac{\vec{F}}{m_c}$$

(2.23)

The relative motion between the two satellites will be:

$$\ddot{\vec{s}} = \ddot{\overrightarrow{r_c}} - \ddot{\overrightarrow{r_t}}$$

(2.24)

Since the purpose is to represent the roto-translational motion of the chaser in the rotating target local frame, linearizing $\overrightarrow{f_g}\,(\overrightarrow{r_c})$ around $\overrightarrow{r_t}$ using the Taylor expansion to first order one can obtain the general linear equations for the relative motion known as Hill's equation (for further information regarding the mathematical calculation see *Appendix A* in reference [1]):

$$\ddot{x} - 2\,\omega\,\dot{z} = \frac{F_x}{m_c}$$
$$\ddot{y} + \omega^2\,y = \frac{F_y}{m_c}$$
$$\ddot{z} + 2\,\omega\,\dot{x} - 3\,\omega^2\,z = \frac{F_z}{m_c}$$

(2.25)

The term ω defines the target orbit angular velocity, $\omega = \frac{2\,\pi}{T}$ where T is the period of such orbit which in this case is constant since the orbit is circular.

The same system of equations can be written in a state space representation so it can be used later for simulation purposes inside the MATLAB/Simulink environment. The general form is:

$$\dot{\boldsymbol{x}} = \boldsymbol{A}\,\boldsymbol{x} + \boldsymbol{B}\,\boldsymbol{u}$$

(2.26)

The state vector $\boldsymbol{x}$ contains the position vector $\boldsymbol{r} = [\,x, y, z\,]^T$ and the velocity vector $\dot{\boldsymbol{r}} = [\,\dot{x}, \dot{y}, \dot{z}\,]^T$, $\boldsymbol{A}$ is the state matrix, $\boldsymbol{u}$ is the input vector and $\boldsymbol{B}$ is the input matrix.

$$\begin{bmatrix} \dot{x} \\ \dot{y} \\ \dot{z} \\ \ddot{x} \\ \ddot{y} \\ \ddot{z} \end{bmatrix} = \begin{bmatrix} 0 & 0 & 0 & 1 & 0 & 0 \\ 0 & 0 & 0 & 0 & 1 & 0 \\ 0 & 0 & 0 & 0 & 0 & 1 \\ 0 & 0 & 0 & 0 & 0 & 2\,\omega \\ 0 & -\omega^2 & 0 & 0 & 0 & 0 \\ 0 & 0 & 3\,\omega^2 & -2\,\omega & 0 & 0 \end{bmatrix} \begin{bmatrix} x \\ y \\ z \\ \dot{x} \\ \dot{y} \\ \dot{z} \end{bmatrix} + \begin{bmatrix} 0 & 0 & 0 \\ 0 & 0 & 0 \\ 0 & 0 & 0 \\ \frac{1}{m_c} & 0 & 0 \\ 0 & \frac{1}{m_c} & 0 \\ 0 & 0 & \frac{1}{m_c} \end{bmatrix} \begin{bmatrix} F_x \\ F_y \\ F_z \end{bmatrix}$$

(2.27)

2.5 Rendezvous Maneuvers

This section will explain the maneuvers utilized during the two rendezvous' phases, the far range and the close one, that will be later used during the simulations. As said in the introduction chapter, these maneuvers are modelled in a relative motion using the Hill's equations, so they are true in the limitations imposed by the validity condition of such equations.

2.5.1 Long Range Rendezvous

When this phase of the mission starts, the chaser is located into a lower orbit and still behind the target. One possibility to make it move forwards, towards the target, while also reaching a higher orbit, is to apply a tangential boost. Applying a tangential impulsive thrust leads to an impulsive starting velocity ΔV_{x1} along the V-bar. After one target's orbital period T the spacecraft will cover a distance of

$$\Delta x = \frac{6\,\pi}{\omega}\,\Delta V_{x1}$$

(2.28)

With $\omega = \frac{2\,\pi}{T}$. In order to stop the satellite a new ΔV but in the opposite direction must be applied:

$$|\Delta V_{x1}| = |\Delta V_{x2}| = \frac{\omega}{6\,\pi}\,\Delta x = \Delta V$$

(2.29)

The total impulse needed for is:

$$\Delta V_{total} = \frac{\omega}{3\,\pi}\,\Delta x$$

(2.30)

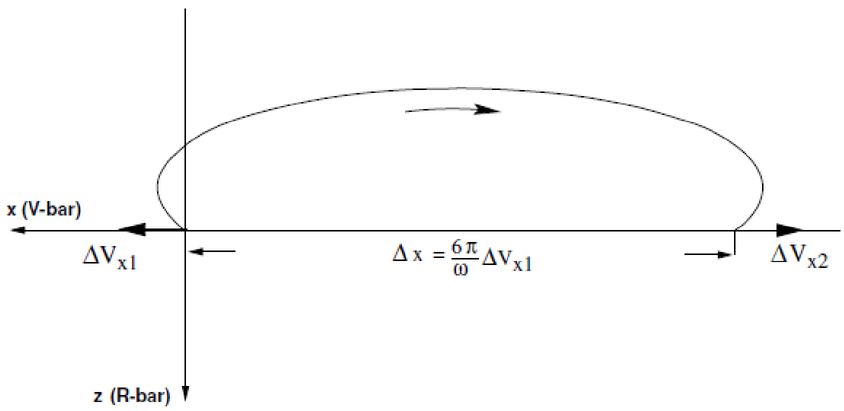

Figure 2.11 – Transfer along the V-bar with a tangential impulse [1]

The maximum high reached by this maneuver is

$$\Delta z = \frac{4}{\omega}\,\Delta V$$

(2.31)

If one needs to reach a higher orbit using a tangential boost it is possible using the same maneuver described before but stopping it at $t = \frac{T}{2}$ thus applying the same impulse equal in size and direction. The new reached orbit will be also circular. During the transfer, the chaser moves along an eccentric orbit and when the second impulse is fired, the orbit returns circular. In this new orbit the satellite moves in a free drift motion. This maneuver is known as Hohmann transfer. At the instant $t = \frac{T}{2}$, the chaser travels for

$$\Delta x = \frac{3\,\pi}{\omega}\,\Delta V$$

(2.32)

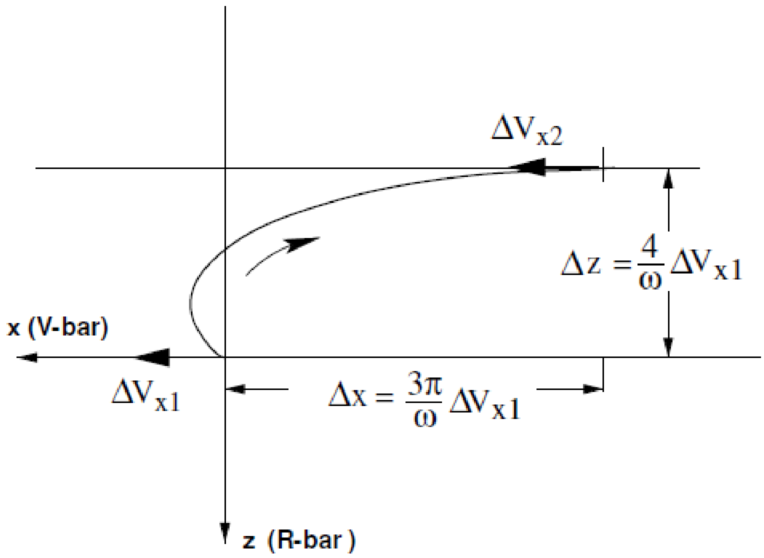

Figure 2.12 – Hohmann transfer [1]

Being the purpose of the Hohmann transfer the orbit change, it is convenient to express the total needed impulse with respect to the Δz desired. From (2.31) it is possible to obtain the amount of one impulse, so the total one is

$$\Delta V_{total} = \frac{\omega}{2}\,\Delta z$$

(2.33)

The total amount of impulse is not sustainable by a small spacecraft like a CubeSat which is not able to attain such a high impulsive boost. In cases like this it is used a continuous thrust instead. The maneuver is now performed by the application of a constant acceleration during the whole duration of it. In this case the only acceleration needed is along the V-bar, γ_x. After a generic amount of time *t*, the amount of ΔV applied considering an acceleration γ_x

$$\Delta V = \gamma_x\, t$$

(2.34)

The drawback of using a continuous V-bar thrust transfer is that it takes the double of time than its impulsive counterpart, so $t = T = \frac{2\pi}{\omega}$. Substituting this value in (2.34) and then substituting the obtained value of ΔV in (2.33) it is possible to obtain the acceleration needed to transfer the satellite in the desired orbit

$$\gamma_x = \frac{\omega^2}{4\pi} \Delta z$$

(2.35)

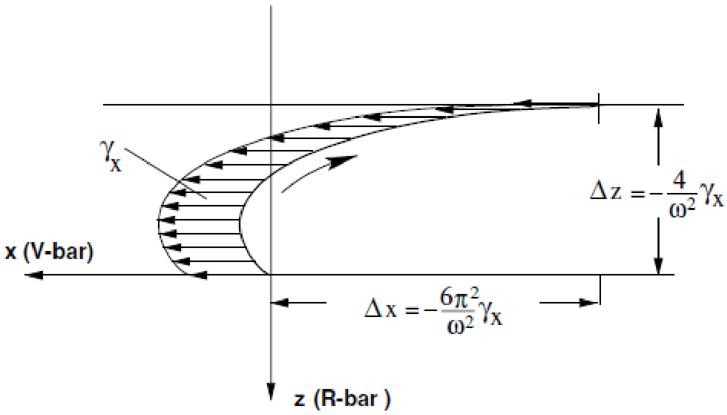

Figure 2.13 – Orbit change with a continuous thrust [1]

It is worth noting that the total amount of ΔV is the same in both cases, the only difference is the time that the two maneuvers require [1].

2.5.2 Short Range Rendezvous

During this phase, the chaser must accomplish some maneuvers close to the target, to shorten its distance and eventually starting the mating phase. In order to perform these maneuvers with a certain safety, a radial boost is chosen.

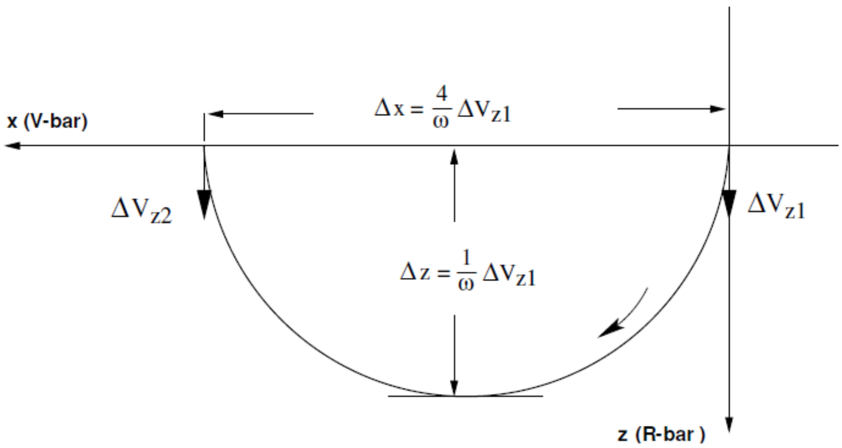

Figure 2.14 – Transfer along the V-bar with a radial impulse [1]

The time needed to transfer the satellite from the position x_1 to the position x_2 is half the period of the orbit. A first impulse is fired to start the maneuver and after $\frac{T}{2}$ a second one, with the same intensity and direction along the R-bar, is shot to stop the satellite. The impulse in the R-bar that must be applied is

$$\Delta V_z = \frac{\omega}{4}\,\Delta x \tag{2.36}$$

The overall ΔV required will be

$$\Delta V_{total} = \frac{\omega}{2}\,\Delta x \tag{2.37}$$

For the same reason shown before, a high impulse is not achievable by a CubeSat, thus also in this case a continuous thrust is needed. The time needed is doubled so

$$\Delta V = \gamma_z\,\frac{2\,\pi}{\omega} \tag{2.38}$$

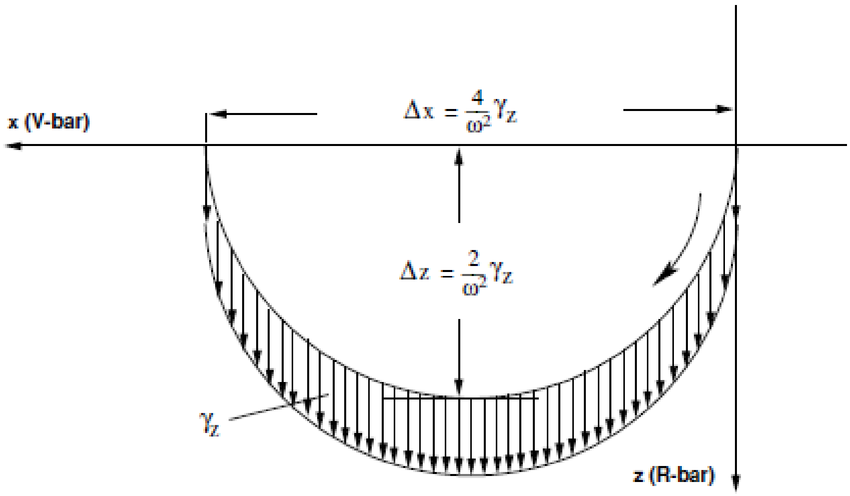

Figure 2.15 -Transfer along the V-bar with a continuous radial thrust [1]

Substituting (2.38) in (2.37) one can obtain the acceleration along the R-bar requested to accomplish the V-bar transfer with a continuous radial thrust

$$\gamma_z = \frac{\omega^2}{4\,\pi}\,\Delta x \tag{2.39}$$

In this case also the ΔV_{total} are equal, the difference lies in the time that has elapsed.

Comparing (2.37) and (2.30) one can notice that the radial impulse maneuver needs a total ΔV bigger than the tangential one, by a factor of $\frac{3\,\pi}{2}$. This results in a higher fuel consumption.

What makes this maneuver more attractive in this particular phase of the mission is its intrinsic safety aspect. If for any reason the second impulse may not occur, in absence of other disturbances, the satellite continues its circular motion returning to its initial position after one orbital revolution without reaching a position farther than x_2. This means that if one wants to retry the maneuver this happens with no extra ΔV to reposition the chaser. This does not happen in the presence of a tangential boost in which, without the second impulse, the satellite continues to advances in the V-bar direction, putting at risk the mission with an hypothetical collision between the chaser and the target [1].

2.6 Control System

Control theory aims to control a dynamic system by developing an algorithm capable to drive it to a desired state. In doing so a closed-loop system is used since it allows, by means of a feedback branch, to compare the actual state of the system with the desired one. The objective is to reduce the resulting error given by this difference. The modern approach is based on the state-space representation of the system to control, which in this application is the one reported in (2.27).

2.6.1 Attitude Control

The chaser is modelled as a rigid body with a shape of a parallelepiped having dimension $l_x =$ 30 cm, $l_y = l_z =$ 10 cm and a mass $m_c =$ 4 kg. From (2.11), the inertia matrix of the satellite is

$$I = m_c \begin{bmatrix} \frac{{l_y}^2 + {l_z}^2}{12} & 0 & 0 \\ 0 & \frac{{l_x}^2 + {l_z}^2}{12} & 0 \\ 0 & 0 & \frac{{l_x}^2 + {l_y}^2}{12} \end{bmatrix}$$
$$= \begin{bmatrix} 0.00667\ kg\ m^2 & 0 & 0 \\ 0 & 0.03333\ kg\ m^2 & 0 \\ 0 & 0 & 0.03333\ kg\ m^2 \end{bmatrix} \tag{2.40}$$

This body has its own state $\boldsymbol{x} = (\boldsymbol{q}, \boldsymbol{\omega})$ that depends on its orientation $\boldsymbol{q}$ and its angular velocity $\boldsymbol{\omega}$, expressed in its body frame. Recalling the quaternion kinematic equation and the Euler dynamic equation:

$$\begin{aligned} \dot{\boldsymbol{q}} &= \frac{1}{2}\, Q\, \boldsymbol{\omega} \\ \dot{\boldsymbol{\omega}} &= -I^{-1}\, \boldsymbol{\omega} \times I\, \boldsymbol{\omega} + I^{-1}\, \boldsymbol{u} \end{aligned} \tag{2.41}$$

Where the matrix Q is already defined in (2.21), $\boldsymbol{u}$ is the output of the controller, which in this case represent a moment and the operation $\boldsymbol{\omega}\, \times$ can be described as follow

$$\boldsymbol{\omega} \times = \begin{bmatrix} 0 & -\omega_3 & \omega_2 \\ \omega_3 & 0 & -\omega_1 \\ -\omega_2 & \omega_1 & 0 \end{bmatrix}$$

(2.42)

To goal of the controller is to reduce the difference between the actual state and a reference vector $(\boldsymbol{q_r}, \boldsymbol{\omega_r})$. The error that exists between these quantities is

$$\begin{aligned} \widetilde{\boldsymbol{\omega}} &= \boldsymbol{\omega_r} - \boldsymbol{\omega} \\ \widetilde{\boldsymbol{q}} &= \boldsymbol{q}^{-1} \otimes \boldsymbol{q_r} = \boldsymbol{q}^{*} \otimes \boldsymbol{q_r} \end{aligned}$$

(2.43)

Where $\boldsymbol{q}^{*} = \begin{bmatrix} q_0 \\ -\boldsymbol{q_v} \end{bmatrix}$ represents the quaternion conjugate [17].

It is possible now to define the control law. In this thesis two different methodologies for the attitude controller are tested: Sliding Mode Control (SMC) for the long range rendezvous and Linear Quadratic Regulator (LQR).

2.6.1.1 Sliding Mode Controller

The Sliding Mode Control is a methodology widely used for non-linear system. It has a solid mathematical base which permits to be robust against disturbances, noises, and uncertainties. It is based on two fundamental steps: the definition of what is called sliding surface and the design of the control law capable to bring the state of the system on this surface. The principle affirms that if the trajectory to track is confined to the sliding surface, then the error tends to be zero exponentially [17], so the sliding surface must present two important characteristic. It must be: invariant, which implies that if the trajectory is on the surface, it remains on it; attractive, if the trajectory is outside the surface then the surface forces the trajectory to move on it. A complete mathematical dissertation can be found in [17] and [18].

A common way to define the surface is

$$s = \widetilde{\boldsymbol{\omega}} + k_2 \, sign(\widetilde{q_0}) \, \widetilde{\boldsymbol{q_v}}$$

(2.44)

Since the surface must be invariant, its derivate should be zero

$$\dot{s} = \dot{\boldsymbol{\omega}}_r + I^{-1} \boldsymbol{\omega} \times I \boldsymbol{\omega} - I^{-1} \boldsymbol{u} + \frac{k_2}{2} \left(|\widetilde{q_0}| \, \widetilde{\boldsymbol{\omega}} + sign(\widetilde{q_0}) \widetilde{\boldsymbol{q_v}} \times (\boldsymbol{\omega}_r + \boldsymbol{\omega}) \right) = 0$$

(2.45)

Solving with respect to $\boldsymbol{u}$, it is possible to find the control law that makes the surface invariant

$$\boldsymbol{u_s} = I \left(\dot{\boldsymbol{\omega}}_r + \frac{k_2}{2} \left(|\widetilde{q_0}| \, \widetilde{\boldsymbol{\omega}} + sign(\widetilde{q_0}) \widetilde{\boldsymbol{q_v}} \times (\boldsymbol{\omega}_r + \boldsymbol{\omega}) \right) \right) + \boldsymbol{\omega} \times I \boldsymbol{\omega}$$

(2.46)

A discontinuous term is added to make it also attractive. Usually is used a sigmoid function which attenuates the chattering problem. The final control law will be

$$\boldsymbol{u} = \boldsymbol{u_s} + k_1 I \tanh(\eta s) \tag{2.47}$$

2.6.1.2 Linear Quadratic Regulator

2.6.2 Position Controller

2.7 Control allocation

2.8 Modulator

Chapter 3

Simulation and results

The simulations involve the use of two different thrusters configurations, an ideal one and a more realistic one.

The ideal configuration is based on a cluster composed by six thrusters, arranged along the principal axes of inertia of the chaser, each thruster is responsible for the motion along one direction of the axis.

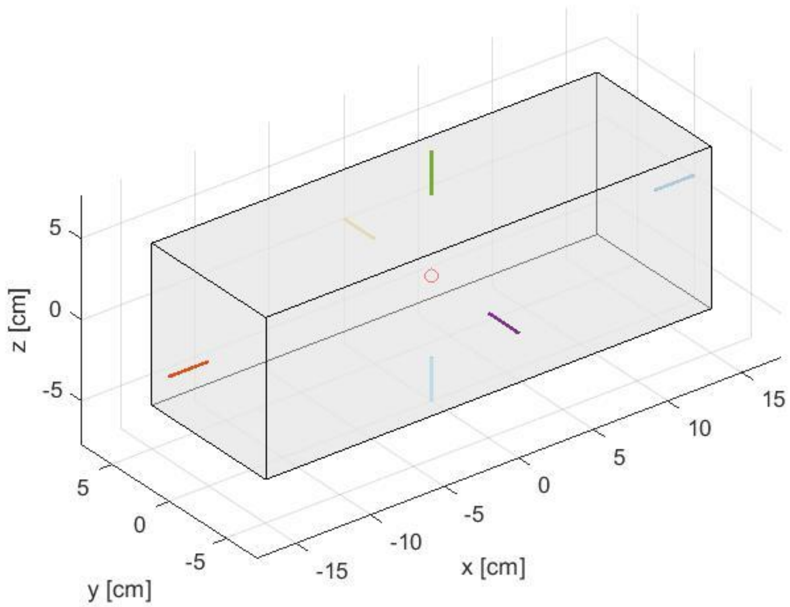

Figure 3.1 – Ideal six thrusters configuration

The real configuration presents a cluster composed by seven thrusters, in which the actuators can also change the orientation of the satellite.

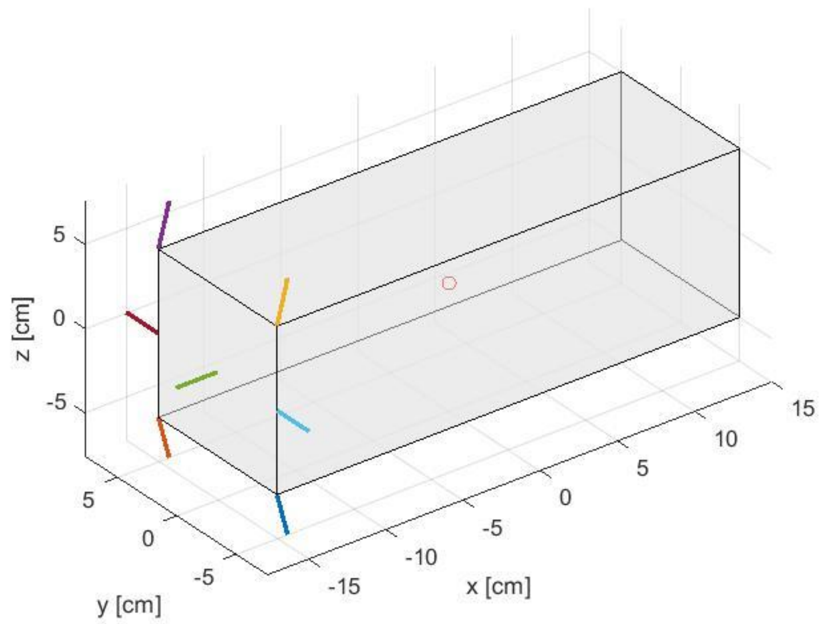

Figure 3.2 – Real seven thrusters configuration

The motion of the chaser is described with respect to the target centered frame since during the rendezvous maneuvers a relative navigation measurement of the states is used.

3.1 Long Range Rendezvous

During the far range rendezvous, the chaser tracks the reference trajectory given by the Hohmann transfer orbit. It starts its maneuver in a lower orbit, 2 km under the target and 6.7 km behind it. At the beginning of the maneuver, it presents an angular velocity. The attitude controller must stop its rotation bringing its attitude to the desired one.

The chaser applies a tangential continuous thrust to raise its orbit while shorten its distance from the target, reaching the final position in a station keeping point 300 m behind the target and 50 m under. This point will be the starting position for the close-range rendezvous.

The system is tested with three different control allocation algorithms and without it to make a comparison of the fuel expense during the maneuver. The modeling of thrusters is made more real by means the design of a modulator to simulate the ON/OFF nature of the actuators. The fuel expense is evaluated indirectly analyzing the total ΔV requested to accomplish the orbit transfer since it is strictly related to the fuel consumption by the Tsiolkovsky rocket equation.

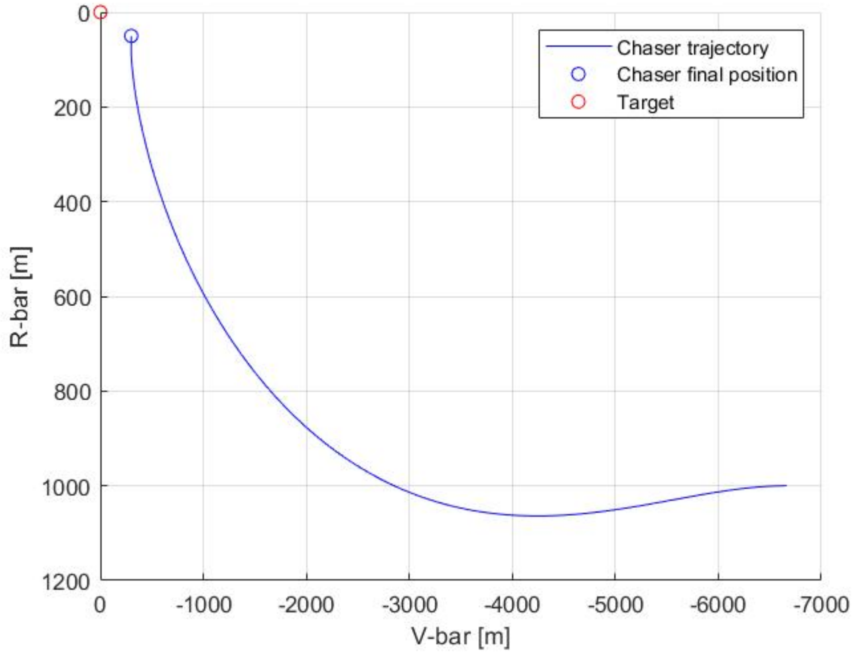

Figure 3.3 – Far range rendezvous

The two configurations, has expected, have shown different performances. Due to the peculiar configuration of the 7-thrusters chaser, the coupling effect of the thrusters, made more difficult to stabilize the satellite, resulting in more firing shoot.

Algorithms and thruster configuration used	**Total ΔV [m/s]**
No control allocation	0.74415
6-thrusters Pseudo Inverse	0.73535
6-thrusters Linear Programming	0.73535
6-thrusters Quadratic Programming	0.73425
7-thrusters Pseudo Inverse	0.94105
7-thrusters Linear Programming	0.94160
7-thrusters Quadratic Programming	0.93858

Table 1 – ΔV expense for the Hohmann transfer

From Table 1 it is possible to see that, in the ideal case, there is an improvement in the management of the fuel.

Both the thruster managed to accomplish the maneuver and to stabilize the chaser in the desired orientation.

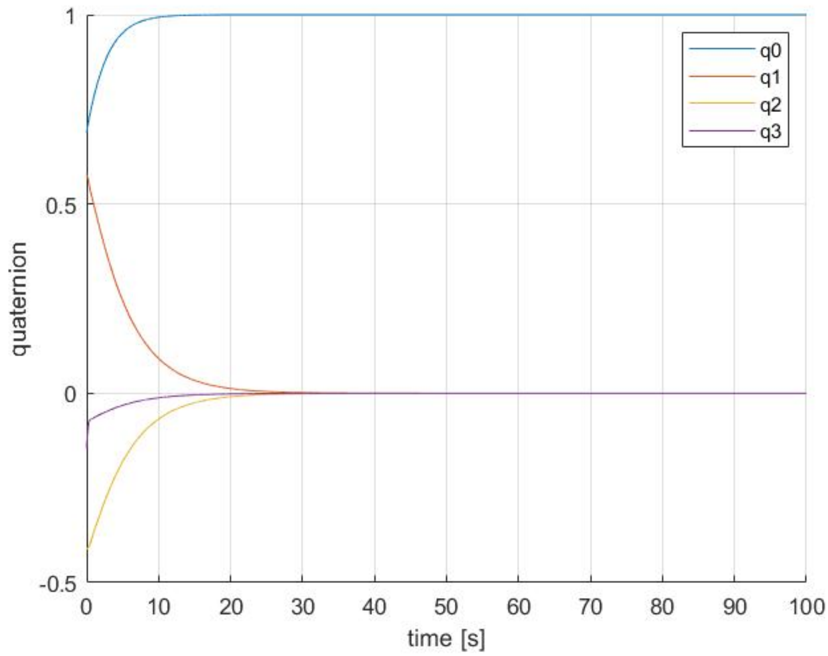

Figure 3.4 – Quaternion stabilization

The stabilization occurred with different moments application between the two satellites, that is because of the coupling effect mentioned before.

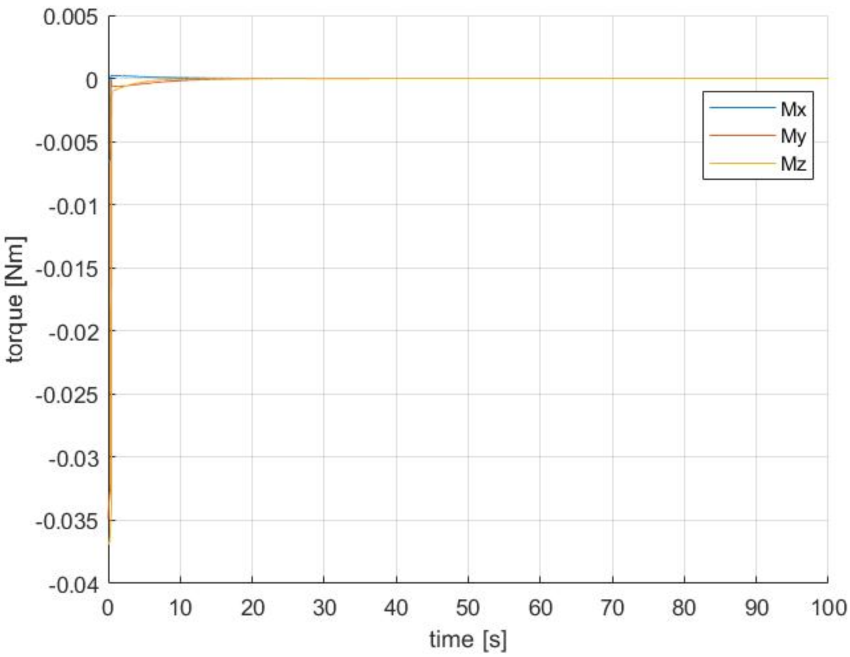

Figure 3.5 – Resulting torques of the six thrusters satellite

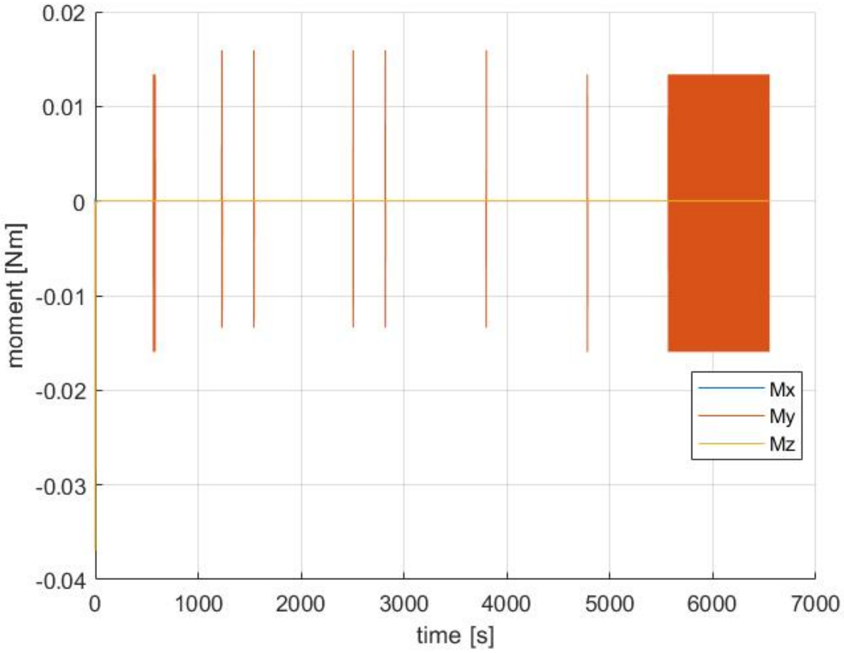

Figure 3.6 – Resulting torques of the seven thrusters satellite

From Figure 3.5 it can be seen that, except for the initial torques needed to bring the satellite to the desired attitude, there are no longer interventions by the attitude controller. On the other hand, in the seven thrusters satellite, due to the coupling effect, the controller must intervene whenever one of the four thrusters on the vertices of the satellite is fired since to correct the position along the *z* axes they must be fired in pairs, resulting in a moment along the *y* axes.

3.2 Short-range Rendezvous

During the short-range maneuver, the chaser, by means of a series of radial continuous thrusts, reaches several station keeping points and eventually, in case the final position does not respects the safety constraints for starting the mating with the target, it flies back to a previous station keeping point.

Station keeping point	Relative distance from the target [m]
S0	(-300 0 -50)
S1	(-64,38 0 0)
S2	(-50 0 0)
S3	(-15 0 0)
S4	(-3 0 0)

Table 2 – Station keeping point

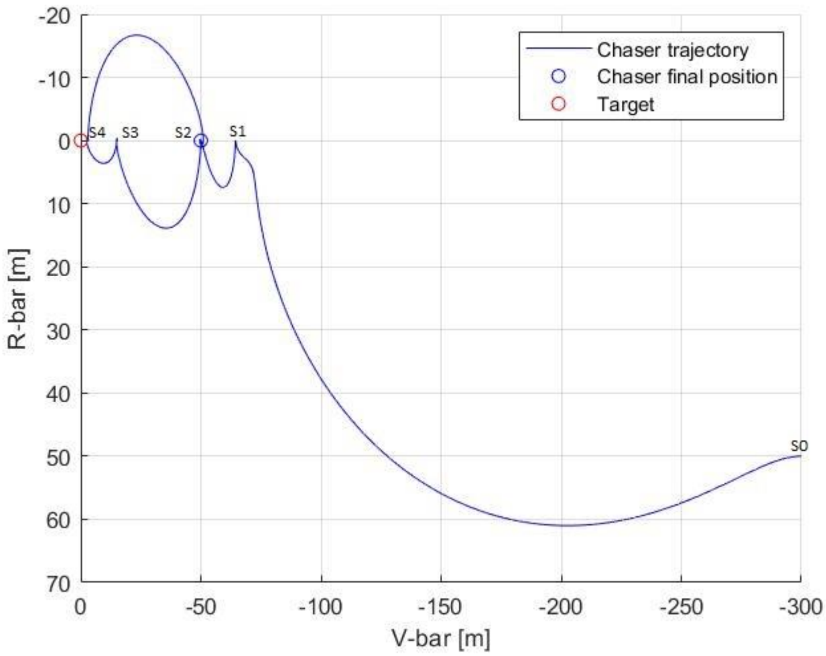

Figure 3.7 – Short-range rendezvous

During this phase only the six thrusters satellite is tested with no PWPF modulator and only two of the three studied control allocator managed to accomplish the maneuver, PI and LP. The use of the seven thrusters configuration, or the modulator, or the QP allocator, resulted in instability inside the system.

Algorithms and thruster configuration used	Total ΔV [m/s]
No control allocation	0,41470
6-thrusters Pseudo Inverse	0,41460
6-thrusters Linear Programming	0,41372

Table 3 – ΔV expense for the short-range rendezvous

In this case, the difference of the fuel consumption, is very small. This can be attributed to the lack of the modulator which, that regulating the number of shoots, is able to lower the activation of the thrusters as it can be seen in Figure 3.8.

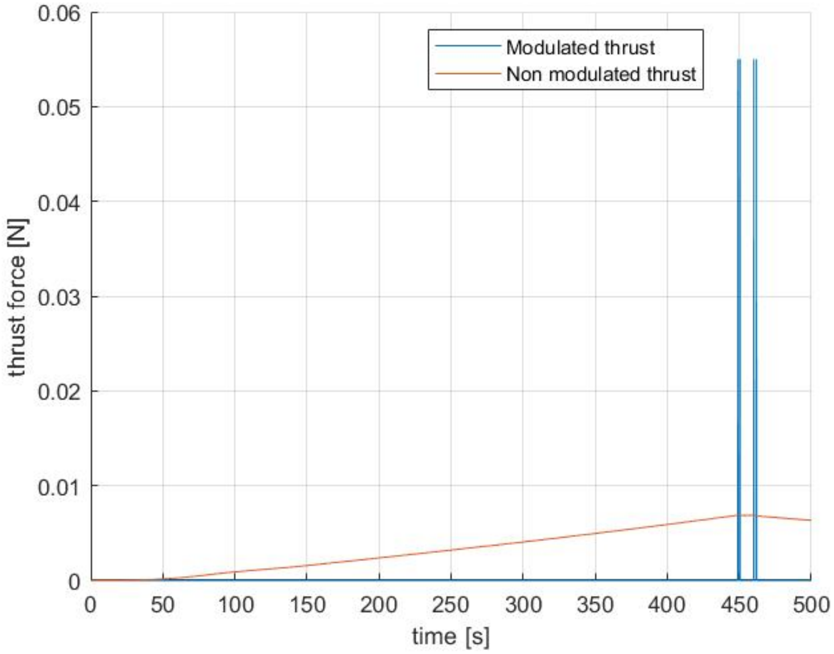

Figure 3.8 – Example of thrust's modulation

In this case the orientation, since the chaser was already stabilized in the desired orientation and, in lack of external disturbances and deriving torques from thrusters' activation, remains the same throughout the duration of the mission.

Chapter 4

Conclusion and future work

Although the 7-thrusters configuration shows a worst performance, one must consider that it presents an almost real disposition of the actuators. Its configuration allows to reorient the satellite using the thrusters along with the reaction wheels responsible for the attitude and more important to desaturate them. The limit of the 6-thrusters configuration is that the satellite can only move along the principal axis of inertia. A combination of control allocation algorithm and controllers can improve the performance in terms of fuel consumption, due to the reduction of ΔV. The tested algorithms have shown the capability to map the command control onto the actuators. They present pros and cons, and the choice of the right allocator depends on the configuration of the thruster, the type of the thruster (if it is unidirectional or no) and on the resource at disposition. Among the three different control allocators, the one based on the QP optimization has shown better results. It must be said though that it needed more time to run with respect to the PI, but, on the other hand, with PI it is not possible to handle the physical constraints of the thrusters. In fact, when a negative value of the force is given as output from the allocator, by means of a redirection system of SIMULINK blocks designed by hand and tailored for the two different configurations, it is redistributed to the thruster in charge of such thrust's direction.

Future works may involve development of better and faster optimization algorithms, especially talking about LP optimization, which also present a more relaxed way to deal with the constraints imposed by the thruster. Other implementations to improve the performance may regard an automatic optimization algorithm to better model the modulator responsible for the ON/OFF of the thrusters. A Particle Swarm Optimization (PSO) algorithm was first used but the attempt failed because of the high demand of memory that the simulation and the iterative procedure of PSO needed.

Bibliography

[1] W. Fehse, *Automated rendezvous and docking of spacecraft*. Cambridge: Cambridge Univ. Press, 2003.

[2] «CubeSat - Deployer standards - eoPortal Directory - Satellite Missions». https://directory.eoportal.org/web/eoportal/satellite-missions/c-missions/cubesat-deployer

[3] «Technology CubeSats». https://www.esa.int/Enabling_Support/Space_Engineering_Technology/Technology_CubeSats

[4] A. Camps, *Nanosatellites and Applications to Commercial and Scientific Missions*. IntechOpen, 2019. doi: 10.5772/intechopen.90039.

[5] W. Lan, «CubeSat Design Specification Rev. 14», pag. 34.

[6] D. Sternberg, J. Essmiller, C. Colley, A. Klesh, e J. Krajewski, «Attitude Control System for the Mars Cube One Spacecraft», in *2019 IEEE Aerospace Conference*, Big Sky, MT, USA, mar. 2019, pagg. 1–10. doi: 10.1109/AERO.2019.8741816.

[7] «InSight Launch Press Kit | Mars Cube One». https://www.jpl.nasa.gov/news/press_kits/insight/launch/appendix/mars-cube-one/

[8] H. Z. I. Khan, J. Rajput, S. Ahmed, M. Sarmad, e M. Sharjil, «Robust control of overactuated autonomous underwater vehicle», pag. 7.

[9] H. Yang e Q. Hu, «Research and Experiment on Dynamic Weight Pseudo-Inverse Control Allocation for Spacecraft Attitude Control System», in *2019 Chinese Control Conference (CCC)*, Guangzhou, China, lug. 2019, pagg. 8200–8205. doi: 10.23919/ChiCC.2019.8865693.

[10] M. Bodson, «EVALUATION OF OPTIMIZATION METHODS FOR CONTROL ALLOCATION», pag. 29.

[11] Y. Zhang e Z. Chen, «A closed-loop control allocation method for satellite precision pointing», in *IEEE 10th International Conference on Industrial Informatics*, Beijing, China, lug. 2012, pagg. 1108–1112. doi: 10.1109/INDIN.2012.6301164.

[12] K. A. Bordignon, «Constrained control allocation for systems with redundant control effectors», Ph.D., Virginia Polytechnic Institute and State University, United States -- Virginia, 1996.

[13] J. Jin, B. Park, Y. Park, e M.-J. Tahk, «Attitude control of a satellite with redundant thrusters», *Aerosp. Sci. Technol.*, vol. 10, n. 7, pagg. 644–651, ott. 2006, doi: 10.1016/j.ast.2006.04.005.

[14] M. Wang e Y. Xie, «Design of the optimal thruster combinations table for the real time control allocation of spacecraft thrusters», in *Proceedings of the 48h IEEE Conference on Decision and Control (CDC) held jointly with 2009 28th Chinese Control Conference*, Shanghai, China, dic. 2009, pagg. 5063–5068. doi: 10.1109/CDC.2009.5400664.

[15] By MathsPoetry - Own work (Personal drawing), CC BY-SA 3.0, https://commons.wikimedia.org/w/index.php?curid=5948979, *Normal situation: the three gimbals are independent*.

[16] By MathsPoetry - Own work, CC BY-SA 3.0, https://commons.wikimedia.org/w/index.php?curid=5949077, *Gimbal lock: two out of the three gimbals are in the same plane, one degree of freedom is lost*.

[17] C. Novara, «Nonlinear control and aerospace applications course slide», *Politecnico di Torino*.

[18] «Sliding mode control: A survey with applications in math | Elsevier Enhanced Reader».